

Evidence for Disorder Induced Delocalization in Graphite

Lucas Casparis¹, Andreas Fuhrer², Dorothée Hug¹, Dominikus Kölbl¹, and Dominik M. Zumbühl¹

¹Department of Physics, University of Basel, Klingelbergstrasse 82, CH-4056 Basel, Switzerland and

²IBM Research, Zürich Research Laboratory, Säumerstrasse 4, CH-8803 Rüschlikon, Switzerland

(Dated: October 16, 2021)

We present electrical transport measurements in natural graphite and highly ordered pyrolytic graphite (HOPG), comparing macroscopic samples with exfoliated, nanofabricated specimens of nanometer thickness. The latter exhibit a very large c-axis resistivity ρ_c – much larger than expected from simple band theory – and non-monotonic temperature dependence, similar to macroscopic HOPG, but in stark contrast to macroscopic natural graphite. A recent model of disorder-induced delocalization is consistent with our transport data. Furthermore, Micro-Raman spectroscopy reveals clearly reduced disorder in exfoliated samples and HOPG, as expected within the model – therefore presenting further evidence for a novel paradigm of electronic transport in graphite.

Graphite is a paradigmatic layered material and has been investigated intensively for many decades. The in-plane resistivity ρ_{ab} is rather well described by a simple Drude model. However, the resistivity ρ_c along the c-axis, perpendicular to the graphite basal planes, as well as its temperature dependence $\rho_c(T)$, are not described by the simple band structure model [1, 2], and currently lack theoretical understanding despite extended efforts. The resistive anisotropy $R_A = \rho_c/\rho_{ab}$ is a convenient dimensionless parameter characterizing transport properties.

Carbon atoms in the graphite basal planes are strongly bound by covalent bonds, while much weaker Van der Waals forces bind the graphene sheets along the c-axis. Non-trivial disorder such as stacking faults and crystalline grains result in a mosaic angle and complicate electronic transport. For isotropic disorder, simple band theory [1] predicts $R_A = m_c/m_{ab} \sim 140$, the ratio of the corresponding band masses. This agrees well with measurements in natural graphite (NG) [3, 4]. In highly oriented pyrolytic graphite (HOPG), the anisotropy was found to be much larger, even exceeding 10^4 in some experiments [5, 6]. Moreover, band theory [1] predicts a monotonic metallic temperature dependence for both ρ_{ab} and ρ_c , resulting in a temperature independent anisotropy R_A . This is seen in NG [7], but not in HOPG, where ρ_c is non-monotonic with a maximum around 40 K [5, 6, 8], similar to ρ_c in other layered materials, such as NaCo_2O_4 [9] and Cuprates [10]. A large anisotropy far exceeding 100 combined with the non-metallic temperature dependence – together referred to as anomalous behavior – are currently not understood and present a fundamental problem in condensed matter physics [7, 11, 12].

In this work, we use exfoliation and nano-fabrication techniques to investigate both ρ_{ab} and ρ_c (see Fig. 1) in graphite flakes of various thickness in the nanometer range. Remarkably, we find in all types of graphite anomalous behavior – namely a large resistive anisotropy as well as a non-metallic temperature dependence. Previous experiments measure ρ_{ab} only [13]. This permits a comparison of R_A in samples with thicknesses in the

nanometer range with macroscopic samples, which we also prepare and measure. The in-plane resistivity of all samples is in good agreement with reported values [3–5], and shows no size-dependence. Therefore the large R_A in the anomalous samples are to be attributed to a large ρ_c . The measured anisotropies appear consistent with a recent model based on disorder induced delocalization by Maslov *et al.* [14, 15], further corroborated by a disorder characterization of our samples using micro-Raman spectroscopy. Conduction path mixing due to a finite mosaic angle can account for the non-monotonic temperature dependence [16], altogether presenting first experimental evidence for a novel paradigm of electrical transport in graphite.

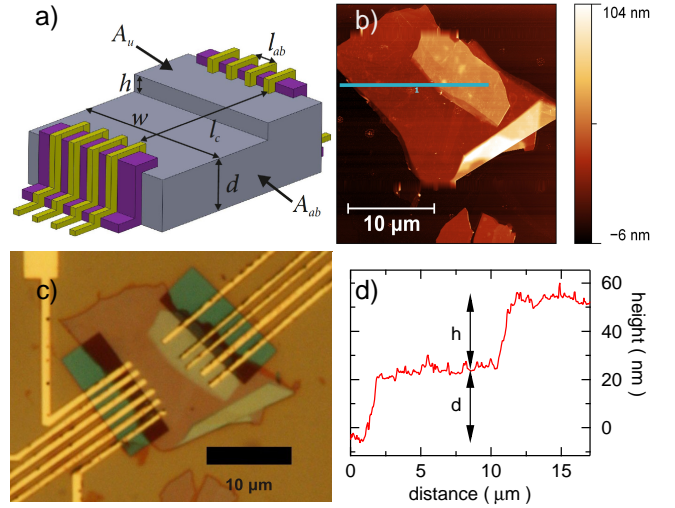


FIG. 1: Nano-graphite samples. (a) Device schematic. Ti/Au contacts (yellow) for 4-wire measurements are patterned on each plateau, isolated from the graphite walls by a SiO_2 layer (purple). AFM picture (b) and optical microscope image (c) of an HOPG flake with two plateaus. (d) Cross section along the blue line in (b), giving plateau heights.

To produce nanostep samples, we use the design shown in Fig. 1(a). We exfoliate graphite onto a Si wafer with a 300 nm thick thermal oxide and identify suitable

flakes with two plateaus differing in height by optical microscopy. The lower plateau height d and the step height h are determined from AFM images [see Fig. 1(b,d)], giving heights between 14 and 150 nm. To extend the range to larger step heights, we use e-beam lithography and oxygen-plasma etching to carve steps up to $h = 450$ nm.

For contacting the plateaus, we first cover parts of the exterior edges of both plateaus with SiO_2 of at least 80 nm thickness [17] in order to prevent short-circuiting the c -axis. Contacts (typically a few hundred nanometers in width) and bonding pads are patterned in a final e-beam step, evaporating a Ti/Au layer thicker than 110 nm (SiO_2 thickness plus 30 nm). A typical device is shown in Fig. 1(c). All resistances are measured with standard 4-wire lock-in techniques. This layout allows measurements of both ρ_{ab} and ρ_c on the same device, as needed to obtain the anisotropy. However, due to variations in the current distribution related to the individual device geometries, corrections to the measured resistances must be applied. We do this by means of a rough estimate based on the simplified geometry shown in Fig. 1(a). In addition, we also performed more elaborate numerical calculations of the current distribution to verify the observed effects [20].

The in-plane resistivity $\rho_{ab} = R_{ab}A_{ab}/l_{ab}$ is estimated from the 4-wire resistance R_{ab} with current and voltage probes on the same plateau and assuming a simple rectangular shape of the graphite sample, with voltage probe distance l_{ab} and total graphite cross section A_{ab} [see Fig. 1(a)]. This is a good approximation for thin, elongated samples, small anisotropy and evenly distributed contacts. For realistic devices as the one shown in Fig. 1(b)+(c) and for large anisotropy, the extracted ρ_{ab} presents an upper bound. Since the current cannot penetrate easily along the highly resistive c -axis and its in-plane distribution is not homogeneous between the current contacts, the effective conduction channel is thinner and narrower than our estimate, thus reducing the actual resistivity below the estimate given here. Nevertheless, the ρ_{ab} extracted (see Fig. 2 and Table I in Ref. [20]) agree rather well with literature [3–5, 18]. Moreover, ρ_{ab} appears independent of the graphite thickness and is similar for NG (from two different sources, Indian NG and Madagascar NG) and HOPG samples, as seen in Fig. 2, open symbols.

Next, we determine the c -axis resistivity ρ_c . Since l_c , the contact to contact distance across the step, is much larger than the step height h (see Fig. 1(a)), we need to subtract the in-plane contributions to the measured resistance R_c to obtain the actual c -axis resistance \widehat{R}_c using

$$\widehat{R}_c = R_c - \rho_{ab} \cdot \left(\frac{l_{cl}}{w_l \cdot d} + \frac{l_{cu}}{w_u \cdot (d + h)} \right), \quad (1)$$

with upper/lower contact to step distance l_{cl}/l_{cu} and corresponding plateau widths w_l/w_u . ρ_c is then obtained from

$\rho_c = \widehat{R}_c A_u / h$, where A_u is the upper plateau area. Depending on the sample geometry, the in-plane correction can be a large fraction of R_c , see supplementary information for an overview. We note that as previously for ρ_{ab} , we again overestimate the thickness d for large anisotropy. However, here, this tends to effectively cancel the overestimated ρ_{ab} , making the extracted ρ_c quite robust. In order to test for the validity of the correction of Eq. 1, we numerically calculate the current distribution for the various contact and sample geometries, taking into account the anisotropy. From a simultaneous fit of the two measurements of R_{ab} and R_c to the calculated resistances we can extract ρ_{ab} , ρ_c and R_A [20]. As anticipated the simulated ρ_{ab} are lower than the approximated ρ_{ab} . For both methods the ρ_c values agree well with each other, corroborating our approach.

Figure 2 displays the resulting ρ_c as a function of height (filled symbols), giving very large ρ_c and correspondingly large anisotropy R_A for all nano-graphites, both NG and HOPG. A power-law fit (linear fit on the log-log graph, slope -1 ± 0.4) through all NG nanostep ρ_c data points seems to indicate a trend of reduction of ρ_c with increasing step height towards the macroscopic ρ_c value in NG samples. HOPG nanostep data is excluded from the fit, since HOPG has no apparent size dependence when going from macroscopic to nanostep samples (filled red diamonds). In order to make a stronger statement, samples with step heights between $1 \mu\text{m}$ and $100 \mu\text{m}$ might give more insight [19].

To allow a comparison with previous experiments, we also investigate macroscopic NG and HOPG samples, again measuring both ρ_{ab} and ρ_c . Due to the geometry used, corrections due to a spreading of the current flow are small and not necessary for the macroscopic samples. On the other hand, the overestimation of the sample thickness due to a large anisotropy is still present, as in previous studies. The values obtained are also added to Fig. 2, together with typical values from literature [3–5]. We find decent agreement between our macroscopic data and previous measurements, reproducing here again the large discrepancy in ρ_c between HOPG and NG in macroscopic samples.

Next, we turn to the temperature dependence $\rho_c(T)$ of the macroscopic samples [21]. For HOPG, we find a non-metallic ρ_c at high T ($d\rho_c/dT < 0$), see Fig. 3 (a). Around 40 K, ρ_c displays a rather shallow maximum, in good agreement with previous HOPG measurements [5]. In contrast, macroscopic Indian NG behaves weakly metallic and monotonic down to 4 K [see Fig. 3 (b)], also in agreement with previous NG data [3]. Overall, our data from macroscopic samples fully agrees with the literature, indicating that our NG and HOPG is of comparable quality to that used in the literature, thus giving us confidence that a comparison of the exfoliated samples with literature is appropriate.

The temperature dependence of the exfoliated nano-

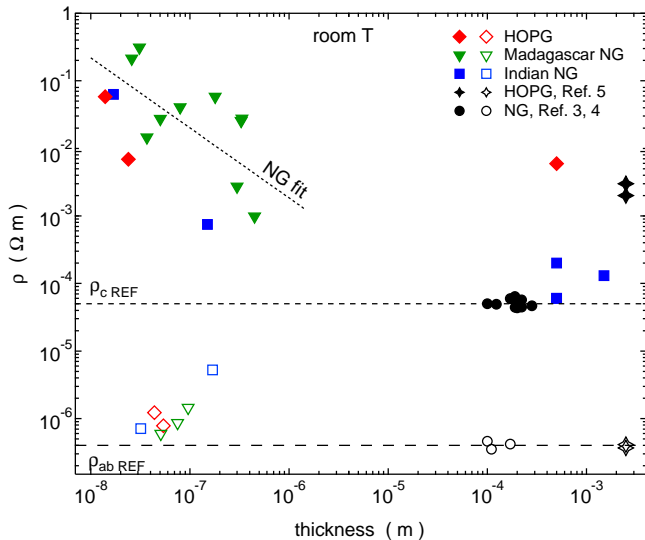


FIG. 2: Influence of graphite thickness on ρ_c (solid markers) and ρ_{ab} (empty markers) at room temperature, comparing HOPG (red) with Madagascar NG (green) and Indian NG (blue). For ρ_{ab} , the abscissa value used is $d + h$, the overall flake thickness, see Table I in Ref. [20]. Previous measurements of macroscopic samples (black) were added for both HOPG [5] (stars) and NG [3, 4] (circles) for comparison. Dashed horizontal lines indicate literature values $\rho_{ab,REF}$ for ρ_{ab} and $\rho_{c,REF}$ for ρ_c . Further, the best power-law fit to all NG nanostep data yields an exponent of -1.0 ± 0.4 and is shown by a dotted line to indicate a potential trend, see text.

graphite samples are shown in Fig. 3 (c) and (d), normalized to the high- T value. In most samples, $\rho_{ab}(T)$ is metallic and monotonous, as expected, and in agreement with macroscopic data [3, 22]. In two specimens, ρ_{ab} exhibits a shallow maximum. This seems to occur occasionally in nanoscale samples, as previously reported [13, 23]. Remarkably, $\rho_c(T)$ of all nanostep samples is qualitatively the same, showing a non-metallic and non-monotonic temperature dependence, qualitatively identical to macroscopic HOPG, and clearly different from the macroscopic NG data. We emphasize that the non-metallic $\rho_c(T)$ combined with the large anisotropy R_A constitutes anomalous behavior for all nanoscale samples. In contrast, only macroscopic HOPG is anomalous, not macroscopic NG.

Motivated by an anisotropy far exceeding the band structure expectation, we consider a recent theory by Maslov et al. [14]. A similar effect was also previously observed for photons [15]. Within this theory, c -axis transport is strongly suppressed in samples with weak bulk disorder due to 1D Anderson localization along the c -axis induced by randomly spaced barriers (e.g. stacking faults). This gives a very large ρ_c and anisotropy R_A , in absence of strong bulk disorder. However, c -axis localization is destroyed by bulk scattering out of the c -axis direction, leading to reduced ρ_c and smaller R_A . Interestingly, here,

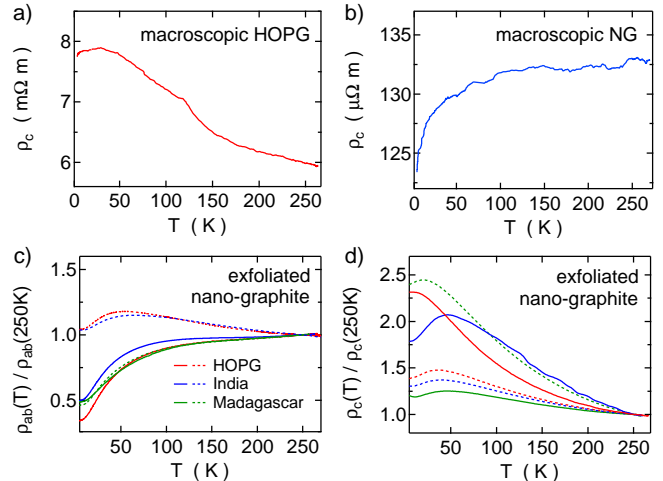


FIG. 3: Temperature dependence of resistivities. $\rho_c(T)$ in macroscopic HOPG (a) and macroscopic Indian (b) NG. (c) $\rho_{ab}(T)$ in nanoscale samples for HOPG (red) and NG India (blue) and Madagascar (green). Two samples are presented for each graphite type (solid, sample 1; dashed, sample 2). For numerical values see Table I in Ref. [20]. (d) $\rho_c(T)$ for the same samples.

disorder can *suppress* Anderson localization, rather than enhancing it, as is usually the case. Therefore, HOPG and nanostep samples are expected to have weak bulk disorder. In contrast, macroscopic NG specimens either have significantly more bulk disorder (suppressing c -axis localization), or fewer c -axis barriers, insufficient for localization (barriers spacing exceeding coherence length).

To characterize disorder, we measure spatially resolved micro-Raman spectra and use the D-peak intensity as a well established measure of graphitic disorder [25, 28]. This peak arises from deviations from the ideal 2D graphene planes with sp^2 bonds, reflecting various types of defects such as dislocations, impurities and other imperfections appearing in bulk graphite [25]. Raman measurements present a characterization of the surface, since the laser ($\lambda = 532$ nm) penetrates only about 50 nm into the bulk graphite [24]. However, several of the nanosamples presented here have step heights less than or comparable to the laser penetration depth. Thus, for such samples, Raman spectroscopy reveals disorder throughout the entire volume of the relevant graphite sections where electron transport along the c -axis occurs – offering a powerful tool to characterize disorder.

To quantify disorder, we introduce the intensity independent and dimensionless quantity $\xi = I_D/I_G$, the ratio of the D-peak intensity I_D and G-peak intensity I_G after subtraction of a constant background. For graphite, one finds $0 \leq \xi \lesssim 1$, where a large ξ indicates a high degree of disorder. At clean locations, the D-peak disappears into the background and its measurement noise, giving $\xi \lesssim 1/50$ corresponding to a D-peak indistinguishable from the noise. We have measured Raman maps of sev-

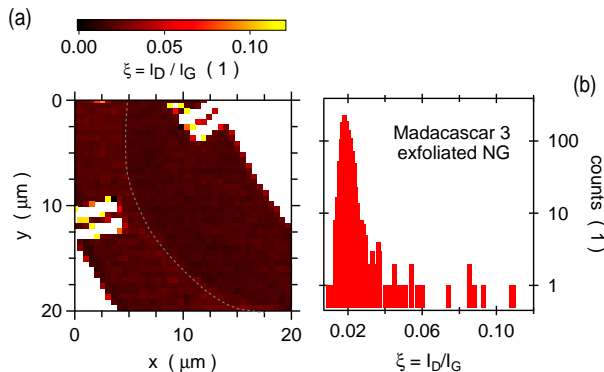


FIG. 4: Disorder characterization with micro-Raman spectroscopy. (a) Ratio $\xi = I_D/I_G$ of the D-peak and the G-peak intensities scanned over an exfoliated Madagascar NG flake (Madagascar 3 [20], scan resolution $\sim 0.5 \mu\text{m}$), with 44 nm tall lower plateau (left) and 31 nm step up (indicated by grey dashed curve) to the upper plateau (right). White is off the graphite flake or on metal contacts. (b) Histogram of ξ for the corresponding scan area.

eral nanostep samples. Figure 4(a) shows a typical scan, from one of the Madagascar samples, displaying only points showing the G-peak characteristic of graphite. We find that disorder is low $\xi \lesssim 1/40$ essentially everywhere away from the edges or contacts, with D-peak within the measurement noise almost everywhere. This is seen on all exfoliated samples we have studied, and agrees well with the model expectations of low bulk disorder in nanostep samples.

The location of the step from the lower to the higher plateau – indicated by the grey dashed curve – leads to only a faint signature in ξ . This arises from a slight change in G-peak intensity at the step [24] and is not visible in the D-peak maps. This suggests that planar defects like stacking faults and grain boundaries may not be readily apparent in Raman scans. Within the model, such planar defects lead to c-axis localization and very large ρ_c in nanosamples with weak bulk disorder as seen here. Thus, these observations are fully consistent with the model.

Exfoliating macroscopic NG even only once already results in strongly reduced surface disorder as seen here by Raman spectroscopy. This is already well known from scanning tunneling microscopy [26]. We have done a control measurements on macroscopic NG samples and find that ρ_c remains low and essentially unchanged after one exfoliation step. Thus, surface disorder is not giving a significant contribution to ρ_c in macroscopic samples.

Finally, we turn to the anomalous temperature dependence of ρ_c . If the c-axis resistivity ρ_c is very large, the c-axis conductance path could easily be mixed with the ab-conductivity σ_{ab} due to a finite mosaic angle θ , effectively short circuiting the intrinsic c-axis conductivity σ_c . Assuming small tilting $\theta \ll 1$, the measured conductivity

$\tilde{\sigma}_c$ can be written as [16]

$$\tilde{\sigma}_c(T) = \sigma_c(T) + \langle \theta^2 \rangle \cdot \sigma_{ab}(T), \quad (2)$$

where $\langle \theta^2 \rangle$ is the variance of θ . In low bulk-disorder samples at low temperatures, the intrinsic σ_c is very small (strongly localized) and $\tilde{\sigma}_c(T)$ obtains a significant component from σ_{ab} , including the (weakly) metallic temperature dependence $\sigma_{ab}(T)$, leading to a slight increase of $\rho_c(T)$ upon increasing T . At higher T , localization is weakened (due to phonon scattering, equivalent to increasing bulk disorder for increasing T), σ_c is enhanced and becomes increasingly more dominant, leading to a decreasing ρ_c above some cross-over T . For both HOPG and NG graphite we measure a mosaic angle between 0.2° and 2° (not shown), which is in agreement with the mixing mechanism, as a mosaic angle of about 0.8° corresponds to a cross-over T of ~ 40 K. For disordered samples, on the other hand, the intrinsic σ_c is dominating $\tilde{\sigma}_c(T)$ since localization is already lifted by disorder, resulting in the usual metallic temperature dependence, as seen in macroscopic NG [7].

This could potentially explain the size dependence mentioned in Fig. 2: thinner samples tend to require more exfoliation steps, therefore becoming cleaner, more localized, and obtaining a larger ρ_c . Ultimately, for sufficiently small h , 1D localization should break down and ρ_c decrease strongly – not visible in the present data, presumably because h is still too large. Overall, the Raman data is consistent with the predictions of the model, namely weak disorder in all exfoliated samples.

In conclusion, we investigate the anisotropy for nanoscale exfoliated graphite, and observe anomalous behavior, namely high ρ_c and non-monotonic $\rho_c(T)$, in both NG and HOPG exfoliated samples. This is in stark contrast to macroscopic samples, where the anomalous behavior is only seen in HOPG, consistent with previous experiments. A recently proposed transport theory [14] can consistently explain this convergence on the nanoscale, the macroscopic data, and the temperature dependence. This adds the nanoscale datapoints to the previously existing macroscopic graphite data. Furthermore, it is consistent with our finding of low disorder in exfoliated and HOPG samples, and high disorder in macroscopic NG. Notably, neutron irradiation experiments inducing bulk disorder have given consistent results [5, 11], i.e. reduced ρ_c after irradiation of HOPG, further corroborating the model. We therefore present clear evidence of disorder induced delocalization, a conceptual novelty, as a new paradigm of electronic transport in graphite.

Though beyond the scope of the present work, it would be very interesting to subject the model to further scrutiny: studying intermediate steps filling the thickness gap in Fig. 2, but also even smaller thicknesses, ultimately down to few- or bi-layer graphene, potentially revealing the localization length. This might be facilitated by bottom contacts with layers deposited on top,

followed by top contacts. We note that the minimum thickness in the present samples is 14 nm, corresponding to about 50 graphene layers. Further, a characterization of graphite disorder would be of great interest, e.g. investigating stacking faults and angles, intercalation, grain and boundary formation [27], aiming at identifying the localization mechanism, leading ultimately to a microscopic understanding of electrical transport in graphite. The results presented here were obtained in graphite, but it would be intriguing to see if similar arguments apply to other layered materials.

We are very grateful to D. Maslov for initiating the experiments and numerous invaluable discussions and to S. Tongay for performing XRD and Raman measurements. Further, we thank F. Dettwiler, D. Maradan and P. Jurcevic for experimental help. This work was supported by the Swiss Nanoscience Institute (SNI), Swiss NSF, ERC starting grant and NCCR QSIT.

-
- [1] S. Ono and K. Sugihara, *J. Phys. Soc. Japan* **21**, 861 (1966).
- [2] K. Sugihara and H. Sato, *J. Phys. Soc. Japan* **18**, 332 (1963).
- [3] W. Primak and L. H. Fuchs, *Phys. Rev.* **95**, 22 (1954).
- [4] L. Edman, B. Sundqvist, E. McRae, and E. Litvin-Staszewska, *Phys. Rev.* **B57**, 6227 (1998).
- [5] I. L. Spain, A. R. Ubbelohde, and D. A. Young, *Phil. Trans. Royal Soc., Series A* **345** (1967).
- [6] T. Tsuzuku, *Carbon* **17**, 293 (1979).
- [7] I. L. Spain, *Chemistry and Physics of Carbon* **19** (1981).
- [8] H. Kempa, P. Esquinazi, and Y. Kopelevich, *Phys. Rev. B* **65**, 241101 (2002).
- [9] T. Valla, P.D. Johnson, Z. Yusof, B. Wells, Q. Li, S.M. Loureiro, R.J. Cava, M. Mikami, Y. Mori, M. Yoshimura, and T. Sasaki, *Nature* **417**, 627 (2002).
- [10] A. N. Lavrov, L. P. Kozeeva, M. R. Trunin, and V. N. Zverev, *Phys. Rev.* **B79**, 214523 (2009).
- [11] B. T. Kelly, *Physics of Graphite*, Applied Science Publisher (1981).
- [12] D. Z. Tsang, and M. S. Dresselhaus, *Carbon* **14**, 43 (1976).
- [13] J. Barzola-Quiquia, J. L. Yao, P. Rodiger, K. Schindler, and P. Esquinazi, *Phys. Stat. Sol. A* **205**, 2924 (2008).
- [14] D. L. Maslov, V. I. Yudson, A. M. Somoza, and M. Ortuno, *Phys. Rev. Lett.* **102**, 216601 (2009).
- [15] S. Zhang, J. Park, V. Milner, and A. Z. Genack, *Phys. Rev. Lett.* **101**, 183901 (2008).
- [16] D. L. Maslov, private communication.
- [17] To accommodate the wide range of sample heights, we take the upper plateau height plus 50 nm as the SiO₂ layer thickness. For the thickest samples, angle evaporation was used additionally to ensure complete coverage of the edges.
- [18] S. Tongay, J. Hwang, D. B. Tanner, H. K. Pal, D. Maslov, and A. F. Hebard, *Phys. Rev. B* **81**, 115428 (2010).
- [19] Producing samples in this range of thickness probably requires a fabrication technique other than exfoliation and presents further technical difficulties.
- [20] see Supplementary Online Material
- [21] In a dip-stick, a calibrated Cernox chip-thermometer was mounted directly adjacent to the sample, ensuring a very similar temperature. The dip stick was moved slowly between liquid ⁴He and the room temperature top flange while continuously measuring both sample and thermometer, resulting in many points in *T*. Cool-down and warm-up curves were measured and compared, giving nearly identical results, and confirming the accuracy of this method. To obtain $\rho_c(T)$, we perform the correction following Eq. 1 at every temperature, using $\rho_{ab}(T)$.
- [22] D. E. Soule, *Physical Review* **112**, 698 (1958).
- [23] Y. B. Zhang, J. P. Small, W. V. Pontius, and P. Kim, *App. Phys. Lett.* **86**, 073104 (2005).
- [24] Y. Y. Wang, Z. H. Ni, Z. X. Shen, H. M. Wang, and Y. H. Wu, *App. Phys. Lett.* **92**, 043121 (2008).
- [25] A. Jorio, M. S. Dresselhaus, R. Saito, and G. F. Dresselhaus, *Raman Spectroscopy in Graphene Related Systems*, Wiley (2011).
- [26] G. Binig, H. Fuchs, C. Gerber, H. Rohrer, E. Stoll, and E. Tosatti, *Europhys. Lett.* **1**, 31 (1986).
- [27] N. Garcia, P. Esquinazi, J. Barzola-Quiquia, and S. Dusari, *New Journal of Physics* **14**, 053015 (2012).
- [28] B. Eren, D. Hug, L. Marot, R. Pawlak, M. Kisiel, R. Steiner, D. M. Zumbühl, and E. Meyer, *Beilstein Journal of Nanotechnology* **3**, 852 (2012).